The Journal of Experimental Biology 205, 999–1007 (2002)
Printed in Great Britain © The Company of Biologists Limited 2002
JEB3809

Modeling an electrosensory landscape: behavioral and morphological optimization in elasmobranch prey capture

Brandon R. Brown*

Department of Physics, University of San Francisco, San Francisco, CA 94117, USA

*e-mail: brownb@usfca.edu

Accepted 19 January 2002

Summary

Most biological sensory systems benefit from multiple sensors. Elasmobranchs (sharks, skates and rays) possess an array of electroreceptive organs that facilitate prey location, mate location and navigation. Here, the perceived electrosensory landscape for an elasmobranch approaching prey is mathematically modeled. The voltages that develop simultaneously in dozens of separate sensing organs are calculated using electrodynamics. These voltages lead directly to firing rate modifications in the primary afferent nerves. The canals connecting the sense organs to an elasmobranch's surface exhibit great variation of location and orientation. Here, the voltages arising in the sense organs are found to depend strongly on the geometrical distribution of the corresponding canals. Two applications for the modeling technique are explored: an analysis of observed elasmobranch prey-capture behavior and an analysis of morphological optimization. For the former, results in specific predator–prey scenarios are compared with behavioral observations, supporting the approach algorithm suggested by A. Kalmijn. For the latter, electrosensory performance is contrasted for two geometrical models of multiple sense organs, a rounded head and a hammer-shaped head.

Key words: electroreception, elasmobranch, prey capture, bioelectric field, hammerhead, evolution, computational neuroethology, modelling.

Introduction

Most biological sensory systems benefit from multiple sensors, and the physical distribution of sensors can play a crucial role in a system's functioning. For instance, the differences detected between two auditory organs lead an animal to locate a sound's source (Rayleigh, 1877; Durlach and Colburn, 1978).

A predator must use sensory input to determine its prey's distance and heading as precisely as possible. The geometry of sensor location can greatly affect this task. Research into the auditory system of predators such as the barn owl, for example, has revealed that bilateral asymmetry in the auditory system – one ear is higher than the other – facilitates prey capture (Volman and Konishi, 1990).

Elasmobranchs can use an electrical sense to locate prey, even in the absence of other cues (Kalmijn, 1966, 1982). Although detailed observations have been made (Kalmijn, 1971, 1982, 1997), a quantitative model for the way in which elasmobranchs 'see' their local electrical landscape has yet to emerge. Here, a mathematical model is used to link quantitatively the physical geometry and movement of an elasmobranch to its resulting neural input.

Some marine elasmobranchs are sensitive to electric fields of less than $5\,\mathrm{nV\,cm^{-1}}$, and they possess hundreds of electrically sensitive organs known as the ampullae of Lorenzini (Kalmijn, 1971; Bennett, 1971). The ampullae are small, innervated bulbs, and these are connected to the aqueous environment by narrow canals terminated by pores. Both the ampullae and the canals are filled with an ion-rich jelly with electrical properties approximating those of sea water (Waltman, 1966). A single canal/ampulla system shows a maximum sensory response when an electric field (voltage gradient) is applied parallel to the canal (Murray, 1962). The ampullae are not sensitive to absolutely static electric fields. Instead, they are sensitive to changes in the electric field that occur in the range 0.1–10 Hz, relevant biological frequencies for prey swimming movements or even gill movements (Montgomery, 1984; Tricas et al., 1995). Since the strength of even a static field emanating from stationary prey will necessarily drop off quickly with distance, a predator approaching the prey will perceive a changing electric field. The relative motion between the observer and the source is the key aspect for the underlying electrodynamics.

Voltages within an ampulla are amplified by ion-channel-mediated interactions between the apical and basal membranes of the ampullary sensing cells (Lu and Fishman, 1994). Sudden voltage changes in the ampullae have been shown to modify firing patterns in the afferent nerves (Murray, 1962; Montgomery, 1984; Wissing et al., 1988; Lu and Fishman,

1994). A sudden drop in voltage within the jelly leads to an increase in the apparent firing rate (excitatory response), while a sudden increase in the jelly voltage leads to a decrease in the measured firing rate (inhibitory response). However, the mapping of voltage to firing rate is not linear, and it can vary from organ to organ (Tricas and New, 1998). Moreover, refined work has shown that the firing rate *per se* does not change, but rather the probability of neuron firing changes (Wissing et al., 1988; Braun et al., 1994).

While the single-organ studies noted above have been very illuminating, an elasmobranch's use of multiple ampullae in mapping its electrical environment remains somewhat mysterious. Some have suggested that the relatively long canals in marine elasmobranchs dampen high-frequency electrical signals (Waltman, 1966). Others have noted that the location of the ampullae and the orientation of their associated canals should be critical to their electric field sensitivity (Bennett and Clusin, 1978). But how does the ensemble of electrosensitive ampullae collaborate to recognize the electric field of nearby organisms? What kind of information do the organs collectively pass to the nervous system?

To link behavior and morphology to actual signals in an elasmobranch's nervous system, I have used electrodynamics to calculate the voltage changes arising at the ampullary ends of the associated canals as a predatory elasmobranch moves near prey. In this way, an approximate picture of body-wide electrosensory input – the electrosensed landscape for the predator – emerges. Since the location and orientation of the canals exhibit great variation both within a single species and among species, and since these geometrical factors influence the results of the calculations, the calculations lend themselves to comparisons of elasmobranch morphology.

After describing the model calculations, the present work uses the technique to address two separate issues. First, certain field observations of elasmobranch feeding patterns are quantitatively evaluated. Second, the modeling technique is used to explore evolutionary optimization by contrasting two elasmobranch morphologies.

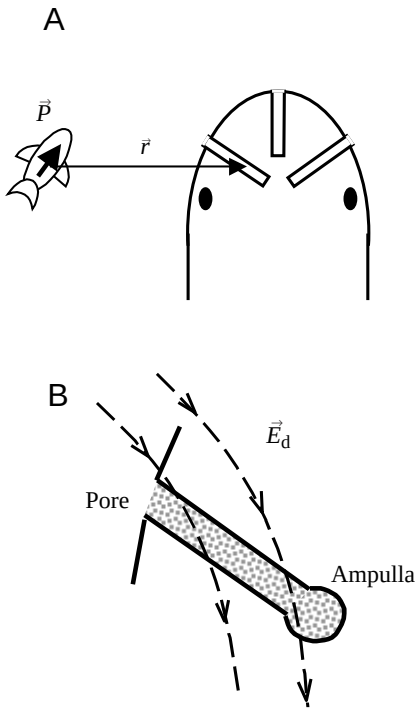

Fig. 1. (A) Dorsal view of simulation geometry. The prey dipole, $\vec{P}$, defines the origin for all calculations. Three sample canals in the elasmobranch are shown for demonstrative purposes. The vector $\vec{r}$ maps out relevant locations in the canals with respect to the prey origin in equation 1. (B) Close-up view of one sensory organ, including the jelly-filled canal that connects a pore to the ampulla of Lorenzini. The electric field ($\vec{E}_d$) of the prey is loosely illustrated by a pair dashed lines. Each canal/ampulla system is described by a vector running from the pore to the ampulla, and its orientation is denoted by the angle measured with respect to the forward direction of the elasmobranch. In A, the sample canals have orientation angles of roughly 130, 180 and 230°. In B, the canal's orientation angle is roughly 130°.

Materials and methods

The model's task is to calculate the change in electric potential at the ampullary end of a canal due to relative motion between a predatory elasmobranch and a prey fish in a two-dimensional (horizontal) space. The model assumes an ideal direct-current dipole field for the prey fish. Although alternating-current components are certainly present, the direct-current field is thought to dominate (Kalmijn, 1971), and higher-order contributions will be of lower magnitude for any separation distance of relevance.

The calculation for one canal is described first. Full simulations then calculate the evolving voltages for 36 such canals. The coordinate system of the calculation is centered on the prey fish (see Fig. 1A). The dipole field emanates from the prey, and a position vector $\vec{r}$ locates any relevant point in the model elasmobranch. A dipole vector $\vec{P}$ represents the electric dipole of the prey fish. The canal, modeled as a vector running from a pore to the corresponding ampulla, is labeled by the angle this vector makes with respect to the forward direction of the predator (upwards on the page). The fact that the label corresponds to canal orientation and not to canal location must be emphasized because a canal's orientation label will often be markedly different from a universal notion of its location. (For instance, in Fig. 1A, the central canal would typically correspond to 0° as a location in the horizontal plane, but the canal vector, running towards the center of the body, would have an orientation of 180° with respect to the forward direction.)

A useful representation of the dipole field for the present task is one that assumes a spatial origin in the center of the dipole and describes the resulting electric field at a distant point ($\vec{E}_d$) in terms of the dipole vector $\vec{P}$ and the separation vector $\vec{r}$:

$$\vec{E}_d = \frac{1}{4\pi\varepsilon}\frac{1}{r^3}\left[3(\vec{P}\cdot\hat{r})\hat{r} - \vec{P}\right], \qquad (1)$$

where $\hat{r}$ is the unit direction vector and r is the magnitude of

the separation vector (Jackson, 1975). This form omits a dirac delta-function at the origin of the field, sensibly restricting the treatment to cases where the elasmobranch is at some non-zero distance from the prey. For simplicity, the calculation uses the static permittivity of sea water, $\varepsilon=7\times10^{-10}\,C^2\,N^{-1}\,m^{-1}$. (A fully dynamic calculation would require the frequency-dependent complex dielectric constant of the jelly that fills the canals and ampullae.) The prey dipole strength is $5.6\times10^{-16}\,C\,m$, giving electric field values consistent with experimental observations of small prey (Kalmijn, 1966).

The canals leading to the ampullae are long (5–20 cm) and narrow (roughly 1 mm across). While the jelly inside conducts reasonably well (the reported electrical resistivity of $24\,\Omega\,cm$ places it within the realm of semiconductors), the walls of the canals are highly resistive (Waltman, 1966). For this reason, the canals can be treated as one-dimensional insulated electrical antennae. For the model, the potential difference (V) between the ampulla and the surrounding sea water is calculated using:

$$V=-\int \vec{E}_d\cdot d\vec{l}, \qquad (2)$$

where $d\vec{l}$ is an infinitesmal segment of the canal and where the integration runs along the canal from the pore to the ampulla (see Fig. 1B). The dot product of the electric field and the canal orientation in equation 2 underlies the physical principle leading to Murray's original observation that a single ampulla gave its sharpest response when its associated canal was parallel to an applied electric field (Murray, 1962). The integral is evaluated numerically by computing the integrand for each 2 cm segment of a canal. This assumes that the electric field strength and direction vary little over a 2 cm displacement and this assumption is robust for prey-to-predator separations of 15 cm or more.

The importance of vector geometry in this simulation contrasts with that required for *Polydon spathula*, the paddlefish, a freshwater electrosensitive predator that has been the subject of recent experiments and modeling efforts (Russell et al., 1999; Greenwood et al., 2000). In the paddlefish, the ampullae are located so close to the skin that only the intensity of the prey's electric dipole field is relevant (Greenwood et al., 2000). Vector geometry also distinguishes our modeling effort from those modeling the sensory input of *Apteronotus albifrons*, a small, weakly electric predatory fish with sense organs on its surface (Nelson and MacIver, 1999). Furthermore, *Apteronotus albifrons* uses active electrolocation, whereas the elasmobranchs use passive electrolocation. This is roughly analogous to the difference between the active echolocation system of a bat and the passive auditory system of the barn owl. Most elasmobranchs must detect the weak electric field of the prey as opposed to an electric response to their own electric field, and the vector nature of the field comes into play as a result of the detailed variation of canal location and orientation.

Since the elasmobranchs appear most sensitive to voltage changes within the range 0.01–10 Hz (Murray, 1962; Montgomery, 1984), the change in the instantaneous voltage (ΔV) is computed between two nearby time points as the ampulla moves with respect to the prey dipole:

$$\Delta V=V(t_0+\Delta t)-V(t_0), \qquad (3)$$

where Δt is the time increment and t_0 is the initial time point. At present, voltage changes are computed over a 0.2 s interval, corresponding to a 5 Hz signal for the elasmobranch. Larger voltage imbalances could build up over longer time scales, certainly, but voltage imbalances within an ampulla are also accommodated (or nulled, effectively) within a few seconds (Murray, 1962; Wissing et al., 1988). Investigating 5 Hz voltage changes specifically avoids both complications. The present study is primarily interested in calculating the relative voltage difference for canals in different locations and different orientations; precise voltage values are of secondary importance. Finding the induced polarity in different organs will show which organs give excitatory responses and which give inhibitory responses.

To calculate the relative differences in potential at the ampullary ends of the canals, a reference potential must be set at the pore end when computing the line integral in equation 2. In keeping with the assumptions of Kalmijn in his treatment of geomagnetic orientation in sharks, the model assumes a potential of zero at the pore (Kalmijn, 1973). This assumes that the sea water electrically 'shorts' the circuit of any two points on an elasmobranch's surface. In fact, the functional model assumption here is much less restrictive. Since this model seeks the change in potential at an ampulla, it assumes only that the potential at an individual pore stays relatively constant over a fraction of a second.

For simplicity, the sea water is assumed to be unmoving. Moving, ion-rich sea water constitutes electric current, and other efforts have convincingly described the way in which an elasmobranch might detect the fields resulting from sea currents (Kalmijn, 1973).

The voltage changes are computed for 36 ampullae simultaneously. Results from two simple predator geometries are presented below. The models (see Fig. 2) are bilaterally symmetrical and purely two-dimensional, and they are intended to explore the utility of the technique more than to reflect exact elasmobranch anatomy. Each model includes an array of 36 straight canals, oriented at intervals of 10° in the horizontal plane. The angles are defined for the vector originating at the pore and terminating at the ampulla, with an angle of zero corresponding to a vector pointing 'north' on the page. Ampullary voltage changes are denoted ΔV_n, where n is the angle index.

Model α, a 'roundhead' elasmobranch, is depicted in Fig. 2A. This can be considered a top view of a predator moving up the page (north). The canal vectors all point inwards and terminate in a cluster of ampullae. All canals in model α have the same length of 10 cm. Admittedly, this model is more symmetrical and uniform than real elasmobranchs. However, actual elasmobranch canal orientations do show nearly 360° of variation, and canals typically have a horizontal component directed away from the skin (Tricas, 2001). In this sense, model

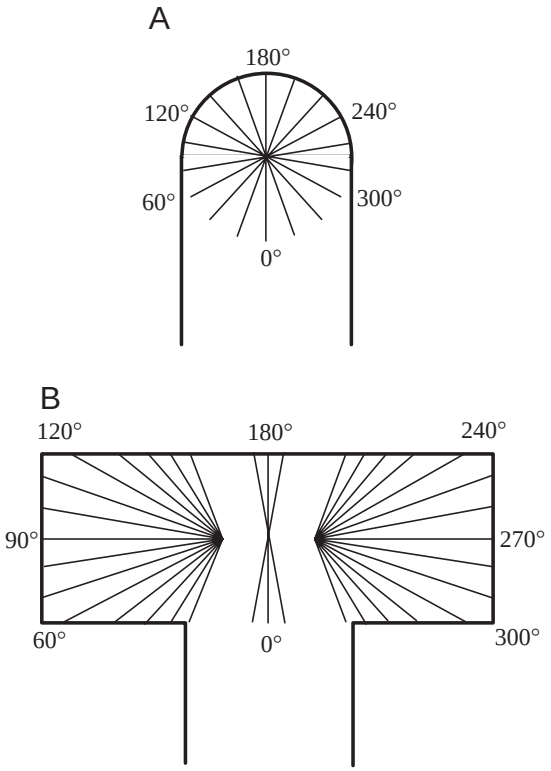

Fig. 2. Elasmobranch models α (A) and β (B). In A, only every other canal and ampulla system is depicted for presentational clarity. Each canal line forms a vector starting on the modeled elasmobranch's surface and terminating at an ampulla inside the model. Model α has one cluster of ampullae; the model measures 20 cm across. Model β has three separate ampullary clusters spaced 5 cm apart; the model measures 50 cm from side to side and 20 cm from front to back.

α is a useful, generic model. It is a sensible starting place for a marine shark or marine ray.

Model β, a 'hammerhead', is shown in Fig. 2B. The hammer geometry is especially well suited for the simulation because it is two-dimensional and it highlights the extreme morphological variation of elasmobranchs. Although still simple and symmetrical, this model is not an unrealistic version of hammerhead canal geometries, particularly for *Sphyrna lewini* (Gilbert, 1967). The model canals vary in length and terminate in three distinct clusters of ampullae. The canal orientations mark out 10 ° intervals exactly like those in model α. The width of the rostrum is 50 cm, and the hammer measures 20 cm from front to back. The sizes of the models are realistic for the heads of sub-adult reef sharks and hammerheads of the same approximate length tip to tail.

Results

Prey-capture approach strategies

The simple case of an elasmobranch directly approaching a prey dipole is calculated first. Here, a stationary prey dipole $\vec{P}$ is oriented at 45 ° east of north, and the elasmobranch model approaches on a northward path as shown in Fig. 3. The

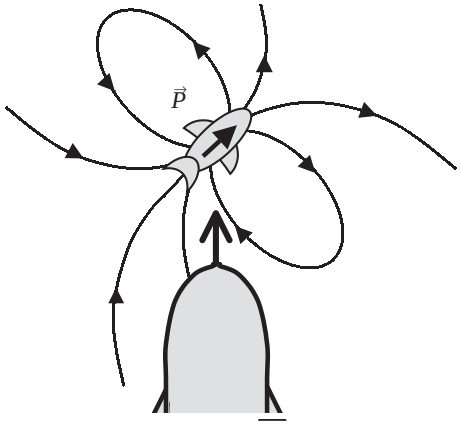

Fig. 3. A model elasmobranch making a straight-line approach to the prey dipole $\vec{P}$, oriented at 45 ° with respect to north. The light lines illustrate the dipole electric field, and the dark vector denotes the approach vector of the elasmobranch.

resulting values of ΔV_n for all ampullae are computed at three sequential points as the elasmobranch closes on the prey.

The voltage changes in the ampullae are plotted in Fig. 4 on the ordinate for the 36 canals, with canals designated by their vector orientation, ranging from 0 to 360 ° on the abscissa. In this picture, 90 ° corresponds to the left side of the predator, 180 ° corresponds to the tip of the rostrum and 270 ° corresponds to the right side. Again, note that the location of the sense organs is typically shifted by 180 ° from the corresponding canal orientation.

Fig. 4A shows the organ-by-organ voltages that develop over 0.2 s when the model moves at 0.5 m s^{-1} through a point located 80 cm to the south of the prey dipole. Similarly, Fig. 4B depicts a later point, when the separation is 50 cm, and Fig. 4C depicts the results when the separation is only 20 cm. Please note that the scale of the ordinate increases by roughly two orders of magnitude from Fig. 4A,B to Fig. 4C (0.1–10 μV scale). In fact, many figures will vary the voltage scale to display the results best.

The basic patterns in Fig. 4 are typical of all such trials for various dipole and elasmobranch orientations. A range of adjacent organs experience positive ΔV_n values, while the others experience negative ΔV_n values.

To reiterate, voltage decreases have been linked to excited firing rates and firing probabilities in the primary afferent nerves of elasmobranchs, while voltage increases have similarly been linked to inhibited firing rates and probabilities (Murray, 1962; Montgomery, 1984; Lu and Fishman, 1994; Braun et al., 1994; Tricas and New, 1998). The modeled ΔV_n in Fig. 4B, for instance, show a maximum change of approximately 75 nV. According to experiments on ampullae excised from skates, a 75 nV voltage rise within the ampulla would lead to an approximately 0.3 % decrease in the firing rate of the primary afferent nerve (Lu and Fishman, 1994). *In situ* measurements show much greater sensitivity of the firing rate to electric field variations. In anesthetized thornback rays, a 75 nV increase would correspond to an almost 2 % change in

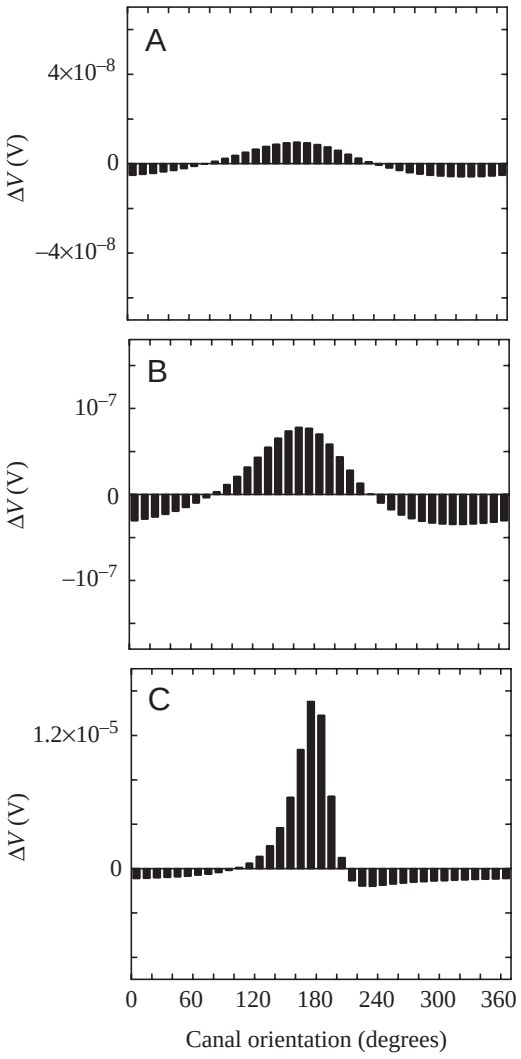

Fig. 4. Voltage changes (ΔV) for 36 canal/ampulla systems for the approach described in Fig. 3. Sequential results for (A) 80 cm separation, (B) 50 cm separation and (C) 20 cm separation.

the firing rate of the primary afferent nerve and, notably, a modification of more than 18 % in the firing rate of the secondary neurons (Montgomery, 1984). More recent measurements on live round stingrays have shown organs with different tiers of sensitivity (Tricas and New, 1998). In the most sensitive organs, a 75 nV increase would correspond to an almost 10 % change in the primary afferent firing rate. The sensitivity of the organs in that study showed dependence on stimulus amplitude. Given the range of results and the apparent non-linearity of rate coding in these organs, the results here will present voltages without a translation to firing rates.

A more complicated and more likely scenario of prey capture is taken up next. Here, the elasmobranch's initial path will not take it directly to the prey. In this case, as shown in Fig. 5, the elasmobranch begins reacting to electrosensory input at point *A*, when it is directly southeast of the prey, 40 cm south and 40 cm east, and moving at 0.5 m s^{-1} to the north. For variety, the dipole is oriented north in this example, parallel to

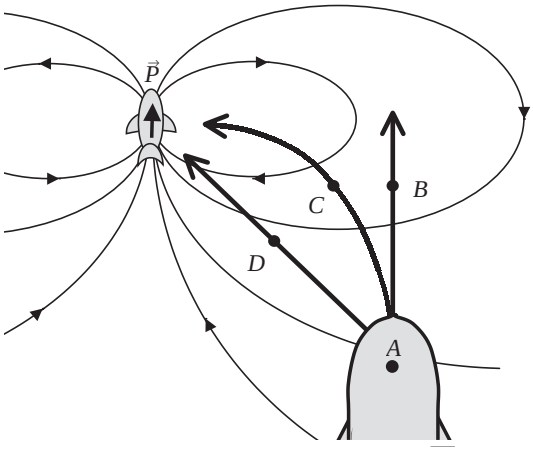

Fig. 5. A model elasmobranch with three approach strategies to a prey dipole ($\vec{P}$) parallel to north. Initially, at point *A* (40 cm east and 40 cm south of $\vec{P}$) the model reacts to the dipole field. Point *B* (40 cm east and 10 cm south of $\vec{P}$) is on the path of the elasmobranch if it were to maintain its original course; point *C* (30 cm east and 10 cm south of $\vec{P}$) is on a path maintaining orientation towards the dipole field; point *D* (20 cm east and 20 cm south of $\vec{P}$) is on the path after an abrupt turn to approach the prey directly.

the elasmobranch's heading. The development of ampullary voltages is computed first at point *A* and then for three predator options: maintaining the original course (path *A* to *B*); moving along a path similar to those recorded in certain behavioral studies, where the elasmobranch maintains a somewhat constant orientation to the dipole field (path *A* to *C*); or turning sharply to take a direct path to the dipole source (path *A* to *D*).

Observationally, Kalmijn collected data for sharks approaching a man-made dipole, so that other senses could presumably be ruled out. He found that *Mustelus canis*, the dogfish, turned and snapped at the dipole source at short range (Kalmijn, 1982). However, he also observed non-direct approaches for both the dogfish and *Prionace glauca*, the blue shark, in which a predator moved along a precise curved path and did not face the prey until just before capture. Both approaches have been observed more recently in *Sphyrna lewini*, the scalloped hammerhead, and *Carcharhinus plumbeus*, the sandbar shark (S. M. Kajiura and T. Fitzgerald, personal communication). Kalmijn (1982) described the non-direct behavior by proposing an 'approach algorithm' in which the predator seeks to maintain a roughly constant angle between its central axis and the local electric field.

Values of ΔV_n in the ampullae of model α were calculated for point *A* and for three options that could possibly follow. Fig. 6A depicts the initial voltage signals to which the elasmobranch model reacts as it moves directly northward. The results for an unaltered course are shown in Fig. 6B; here, the elasmobranch ignores the prey dipole. Results for a path like those observed in *Mustelus canis* are shown in Fig. 6C. (It is actually impossible to maintain the relationship of each canal to the electric field because of the unique gradient of the dipole field; here, at point *C* in Fig. 5, the model has rotated 47 ° counterclockwise, maintaining the relationship of most

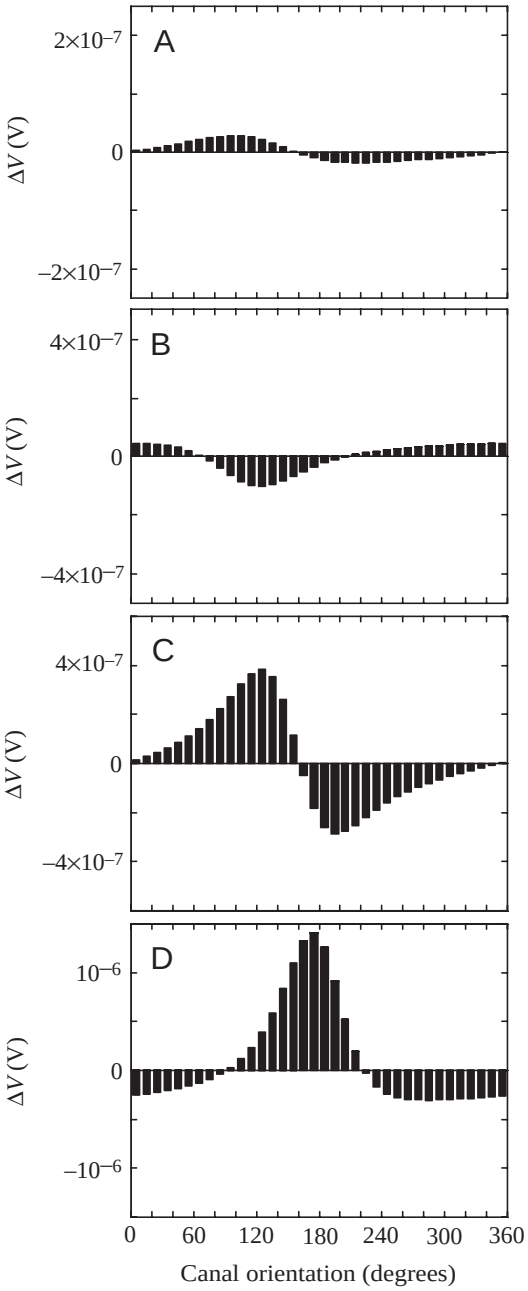

Fig. 6. Voltage changes (ΔV) for 36 canal–ampulla systems for the four points denoted in Fig. 5. Results for (A) the point of first reaction, (B) a model that maintains its initial heading, (C) a model that maintains its orientation to the dipole field and (D) a model that turns to approach the dipole prey directly. Note the changing voltage scales.

canals to the electric field vector to within 5 °.) Results for a quick turn followed by a direct approach are shown in Fig. 6D.

Comparison of morphology

The two models, α and β, were compared and contrasted in two simple predator–prey scenarios.

Fig. 7A,B displays the results of models α and β passing a prey fish to the side. The elasmobranch position in each case is 50 cm west and 15 cm south of the prey dipole. The dipole is oriented at 10 ° east of north, and the elasmobranch moves directly north.

Fig. 7C,D also gives the ΔV_n values that develop in models α and β as they directly approach a prey dipole oriented at 45 ° with respect to north, from a distance of 20 cm. This corresponds to the scenario of Fig. 4C, and the data for model α are replotted for purposes of comparison.

Discussion

Although the models are two-dimensional and several simplifying assumptions have been made, the technique proposed here has shown promise in understanding the electrosensory landscape experienced by marine elasmobranchs. The model links elasmobranch behavior and morphology to approximate sensory input.

The resulting ΔV_n data sketch the sensory input for a creature detecting a vector field. This is novel in that most sensory systems detect scalar information. Olfactory, auditory, thermal and mechanical sensors are all based on the pure intensity of input, whereas the electrical sense attempts to divine both the intensity and the direction of the stimulus. Note the counterintuitive nature of some results. While canals closer to the prey typically give larger signals than the canals on the opposite side of the model rostrum, the data presented in Fig. 7A,B, for example, show relatively small voltages for the organ on the right side (270 °) of the rostrum for both models, even though this organ is one of the closest to the prey fish. The signal is limited because the canal is nearly perpendicular to the dipole field in this case. For a purely intensity-based sense, this organ would register one of the highest voltages.

The basic patterns shown in Figs 4, 6 and 7, an inhibitory electrosensory response from one segment of the rostrum mixed with an excitatory sensory response from another, could be the fingerprint that an elasmobranch learns for nearby organisms.

Prey-capture approach strategies

The modeling results summarized in Figs 5 and 6 offer a sensible explanation for the proposed approach algorithm of Kalmijn (1982, 1987) in which an elasmobranch approaches prey in such a way to maintain a constant orientation to the electric field vector. Note that the forms of Fig. 6A and Fig. 6C are very similar. An animal moving along path *A* to *C* would, after first reacting to the prey electric field at point *A*, simply reinforce the initial firing rate alterations. By loose analogy, an organism can approach a particular sound's source by moving in such a way as to increase the perceived intensity of that sound. Here, the elasmobranch appears to move in such a way as to increase the intensity of a telltale firing pattern from its ampullae.

However, by maintaining its course (path *A* to *B*) or turning to directly approach the prey (path *A* to *D*), the elasmobranch

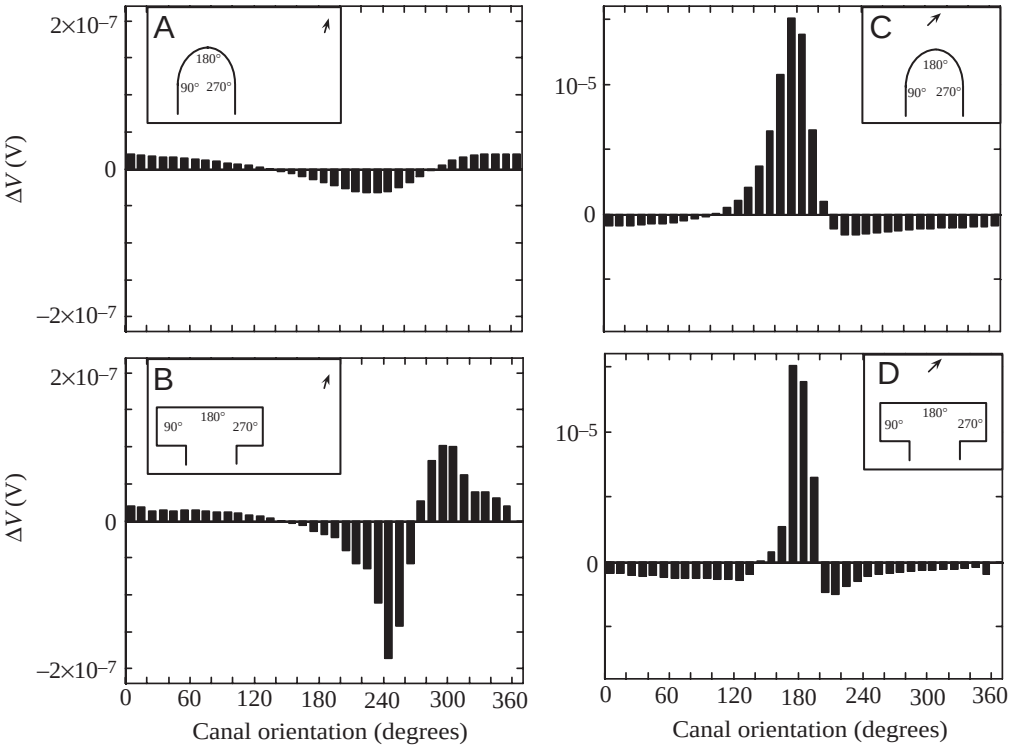

Fig. 7. Comparative signal development for two morphologies. The insets depict the scenario and corresponding model in each case, including reference ampullae orientations. (A,B) Voltage changes (ΔV) in ampullae for models α and β, respectively, as they move north at 0.5 m s^{-1} through a point located 50 cm west and 15 cm south of the prey dipole. The dipole (shown as an arrow) is oriented at 10 ° east of north. (C,D) Voltage changes in ampullae for models α and β, respectively, as they move north at 0.5 m s^{-1} through a point located 20 cm south of a prey dipole. The dipole is oriented at 45 ° east of north.

substantially changes the pattern of ΔV_n. Many organs change their polarity for choices *B* and *D*, so that initially inhibitory responses would become excitatory and *vice versa*. In fact, for the results in Fig. 6B, the organ at 100 ° (almost the left-most organ on the head) has gone from having the maximum positive voltage change (Fig. 6A) to a negative voltage change.

The previous comments offer a qualitative first impression of the data presented in Fig. 6. Ideally, to offer a more quantitative analysis of the results, one would accumulate the firing rate changes from the array of organs, perhaps using a population vector. Such an analysis has been carried out successfully for the sand scorpion *Paruroctonus mesaensis*, a predator that passively collects vibrational data from an array of sensors to locate prey (Sturzl et al., 2000). However, as noted above, rate coding in the elasmobranch's electrosensor is not fully understood, and the population vector is beyond the scope of the initial step presented here.

Instead, behavioral options can be roughly evaluated in a picture of signal reinforcement. A dimensionless measure, *R*, is defined here as a reinforcement factor. It averages the per-organ ratio of initial ΔV_n ($\Delta V_{n,init}$) to final ΔV_n ($\Delta V_{n,final}$), and it weights the importance of each organ by the size of its original voltage signal compared with the average ($\Delta V_{avg,init}$):

$$R = \frac{1}{36}\sum_{n=1}^{36}\frac{\Delta V_{n,final}}{\Delta V_{n,init}} \times \frac{|\Delta V_{n,init}|}{\Delta V_{avg,init}}. \quad (4)$$

While the exact magnitude of a given organ's initial voltage signal, $\Delta V_{n,init}$, cancels from the result, its sign, or polarity, is crucial. An organ that changes its polarity between point *A* and its final position will contribute a negative value to the sum. The weighting factor decreases the significance of organs with tiny voltages and increases the significance of those organs that experience larger than average signals.

Computing this quantity for the data shown in Fig. 6 gives the following. For the unaltered path *A* to *B*, *R*=–1.3; for the direct path *A* to *D*, *R*=–1.1; and for the algorithm path *A* to *C*, *R*=+9.1. These results, together with the numbers of organs maintaining polarity out of 36, are presented in Fig. 8A. Path *A*

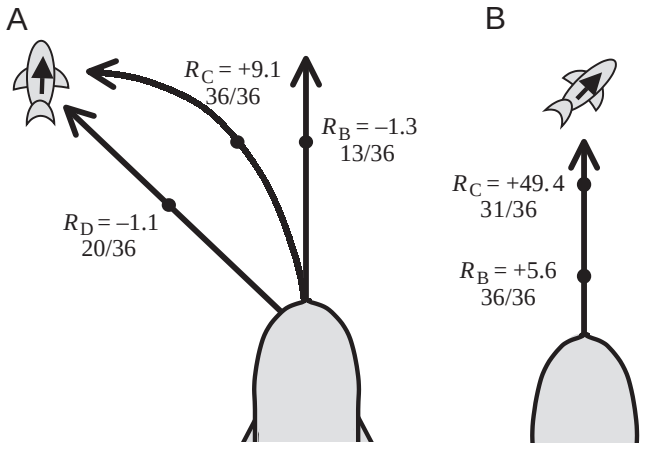

Fig. 8. (A) Quantitative assessment of the reaction paths shown in Fig. 5 for a mathematically modeled elasmobranch. *R*, the reinforcement factor, is defined in the text. The fractions denote the percentage of organs maintaining their initial voltage polarities. (B) Quantitative assessment of the elasmobranch's direct approach to a prey dipole illustrated in Fig. 3.

to *C* gives strong reinforcement of the detected electrosensory signal, with the average organ maintaining its original polarity and increasing the related signal. However, both paths *A* to *B* and *A* to *D* give negative reinforcement values, so that the strong signals typically change polarity. It is somewhat surprising that the turn to a direct approach (which has been observed) is apparently no more beneficial than a path that ignores the signal. Note, however, that the ordinate scales in Fig. 6 show that an animal pursuing path *A* to *D* would receive the largest voltage signals of any option.

To further compare approach strategies depicted by paths *A* to *C* and *A* to *D*, the reinforcement factor is also computed for the simple direct approach shown in Figs 3 and 4. This approach does not involve the quick turn, but otherwise it serves as a sort of intersection of the two observed strategies. When an elasmobranch's initial velocity leads to the prey dipole along a direct radial path (presumably rare if all possibilities are considered), the predator automatically maintains its orientation to the dipole electric field, and this is consistent with the approach algorithm of Kalmijn (1982, 1987). *R* is calculated for the change from 80 to 50 cm and for the change from 50 to 20 cm. The results are shown, again with the number of organs maintaining polarity, in Fig. 8B. Apparently, this path shows dramatic reinforcement of the initial ΔV_n pattern. However, the polarity fraction numbers decrease. As the predator draws close to the prey, some of its organs change polarity, even as the ΔV_n values themselves increase dramatically.

Perhaps the approach algorithm serves as a guide for the predator until, at closer range, it can more precisely determine the prey's exact location. At this point, the algorithm and maintenance of organ polarity are abandoned, and the predator moves as quickly and as directly as possible to the dipole source. Such a detection strategy could help explain the fact that both forms of approach are observed in behavioral experiments. These comments are highly speculative for such a skeletal calculation. In addition to adding computational and morphological complexity, future models of feeding behavior should also consider observed non-linear, pre-detection motions of the predator (e.g. side-to-side movement of the rostrum at a regular frequency).

Comparison of morphology

Although the results for two morphologies display many differences, the qualitative similarity of voltage trends is important in evaluating the modeling technique itself. The induced polarities (positive or negative) of the values of ΔV_n of model β typically match those in the simple rounded model. This is true despite significantly different canal lengths, canal locations and ampullae locations. Since the canal orientations are the only shared characteristic of the two models, the qualitative similarity of the results underscores the importance of canal orientation. Moreover, the similarity increases the confidence with which one can view the results of the behavioral trials discussed above. In short, models more sophisticated than model α give qualitatively similar results. Therefore, the behavioral results above are significant even though model α is more simple and symmetrical than an actual elasmobranch.

Despite the qualitative similarity of ΔV_n patterns for the two models, they also show striking quantitative differences. In the case of Fig. 7B, model β shows substantially greater voltage signals. In fact, the maximum amplitude of voltage change in model β (–185 nV) is approximately six times that found in model α (–30 nV). Referencing data in the thornback ray again, such voltages could correspond to a 0.75 % change in primary afferent nerve firing rates in model α *versus* a 4.5 % change in model β (Montgomery, 1984). This result is not surprising since the hammerhead model places the canals, and some of the ampullae themselves, closer to electric field sources that lie at some distance from the central axis of the elasmobranch. However, model β would also afford an elasmobranch finer angular resolution of the prey location than model α. Note that the largest signal in model β (–186 nV at 240 °) is more than double the signal found in organs only 20 ° away. In addition, the peak stimulus is proportionally much greater than the background for model β. Taking the absolute value of all ampullary signals, the maximum signal in model β is 4.8 times its average ampullary signal (39 nV). Meanwhile, model α has a maximum signal (32 nV) only 2.1 times greater than its average ampullary signal (15 nV).

The results in Fig. 7D also show fine angular resolution in the hammer-shaped model. Although the canals are no closer to the prey source in model β, and the magnitudes of the resulting ΔV_n are no larger, the model again offers better angular resolution than model α. An elasmobranch with sensory organs arrayed along a hammer would evidently have a more precise knowledge of the prey's bearing.

To summarize, the results show a strong quantitative evolutionary advantage for model β over model α. Although many have proposed that the curious hammer shape evolved to aid electroreception, this may be the first detailed, quantitative support for that hypothesis.

The computational technique advocated here shows promise for further morphological comparison. It should be able to illuminate which elasmobranch morphologies are better suited for which electromagnetic task. Future plans for the technique include incorporating greater computing power and digitizing the canal systems of several different elasmobranchs. Such goals appear to be especially well suited for a 'neuroecological' analysis of elasmobranch morphology, and detailed morphological data for the electrosensors of several species have recently appeared in the literature (Tricas, 2001; Kajiura, 2001).

The author thanks Sonya Bahar, Marcelo Camperi, Harvey Fishman, Frank Moss, Mary Hughes, Martin Klinger, David Russell, Chris Smith, Dana Smith, Sean Van Sommeran and an anonymous referee for helpful suggestions, feedback and/or fruitful discussions. This work was supported in part by the Fletcher Jones Foundation and the National Science Foundation through DUE grant no. 87960.

References

Bennett, M. (1971). Electroreception. In *Fish Physiology*, vol. V (ed. W. Hoar and D. Randall), pp. 493–574. New York: Academic Press.

Bennett, M. and Clusin, W. (1978). Physiology of the ampulla of Lorenzini, the electroreceptor of elasmobranchs. In *Sensory Biology of Sharks, Skates and Rays* (ed. E. Hodgson and R. Mathewson), pp. 483–506. Arlington, VA, USA: US Department of Defense.

Braun, H. A., Wissing, H., Schafer, K. and Hirsch, M. C. (1994). Oscillation and noise determine signal transduction in shark multimodal sensory cells. *Nature* **367**, 270–273.

Durlach, N. I. and Colburn, H. S. (1978). Binaural phenomena. In *Handbook of Perception*, vol. IV (ed. E. Carterette and M. Friedman), pp. 365–466. San Francisco: Academic Press.

Gilbert, C. (1967). A taxonomic synopsis of the hammerhead sharks (Family Sphyrnidae). In *Sharks, Skates and Rays* (ed. P. Gilbert, R. Mathewson and D. Rall), pp. 69–78. Baltimore: John Hopkins Press.

Greenwood, P. E., Ward, L., Russell, D. F., Neiman, A. and Moss, F. (2000). Stochastic resonance enhances the electrosensory information available to paddlefish for prey capture. *Physiol. Rev. Lett.* **84**, 4773–4776.

Jackson, J. D. (1975). *Classical Electrodynamics*, pp. 140–141. New York: John Wiley and Sons.

Kajiura, S. M. (2001). Head morphology and electrosensory pore distribution of carcharinid and sphyrnid sharks. *Environ. Biol. Fishes* **61**, 125–133.

Kalmijn, A. (1966). Electro-perception in sharks and rays. *Nature* **212**, 1232–1233.

Kalmijn, A. (1971). The electric sense of sharks and rays. *J. Exp. Biol.* **55**, 371–383.

Kalmijn, A. (1973). *Electro-Orientation in Sharks and Rays: Theoretical and Experimental Evidence*. Scripps Institution of Oceanography Reference Series, Contribution no. 73–39, pp. 1–22.

Kalmijn, A. (1982). Electric and magnetic field detection in elasmobranch fishes. *Science* **218**, 916–918.

Kalmijn, A. (1997). Electric and near-field acoustic detection, a comparative study. *Acta Physiol. Scand.* **161 (Suppl. 638)**, 25–38.

Lu, J. and Fishman, H. (1994). Interaction of apical and basal membrane ion channels underlies electroreception in ampullary epithelia of skates. *Biophys. J.* **67**, 1525–1533.

Montgomery, J. (1984). Frequency response characteristics of primary and secondary neurons in the electrosensory system of the thornback ray. *Comp. Biochem. Physiol.* **79**, 189–195.

Murray, R. W. (1962). The response of the ampullae of Lorenzini of elasmobranchs to electrical stimulation. *J. Exp. Biol.* **39**, 119–128.

Nelson, M. E. and MacIver, M. (1999). Prey capture in the weakly electric fish *Apteronotus albifrons*: sensory acquisition strategies and electrosensory consequences. *J. Exp. Biol.* **202**, 1195–1203.

Rayleigh, J. W. S. (1877). *Theory of Sound*. London: Macmillan.

Russell, D. F., Wilkens, L. A. and Moss, F. (1999). Use of behavioral stochastic resonance by paddlefish for feeding. *Nature* **402**, 291–293.

Sturzl, W., Kempter, R. and van Hemmen, J. L. (2000). Theory of arachnid prey localization. *Physiol. Rev. Lett.* **84**, 5668–5671.

Tricas, T. (2001). The neuroecology of the elasmobranch electrosensory world: why peripheral morphology shapes behavior. *Environ. Biol. Fishes* **60**, 77–92.

Tricas, T., Michael, W. and Sisneros, J. (1995). Electrosensory optimization to conspecific phasic signals for mating. *Neurosci. Lett.* **202**, 129–132.

Tricas, T. and New, J. G. (1998). Sensitivity and response dynamics of elasmobranch electrosensory primary afferent neurons to near threshold fields. *J. Comp. Physiol. A* **182**, 89–101.

Volman, S. F. and Kunishi, M. (1990). Comparative physiology of sound localization in four species of owls. *Brain Behav. Evol.* **36**, 196–215.

Waltman, B. (1966). Electrical properties and fine structure of the ampullary canals of Lorenzini. *Acta Physiol. Scand.* **66 (Suppl. 264)**, 1–60.

Wissing, H., Braun, H. A. and Schafer, K. (1988). Dynamic response characteristics of the ampullae of Lorenzini to thermal and electrical stimuli. *Prog. Brain Res.* **74**, 99–107.